THE JOURNAL OF PHYSICAL CHEMISTRY B

Article

pubs.acs.org/JPCB

Monte Carlo Simulation on Complex Formation of Proteins and Polysaccharides

Yunqi Li,[†,§] Tongfei Shi,[‡,§] Lijia An,[‡,*] and Qingrong Huang[†,*]

[†]Department of Food Science, Rutgers University, 65 Dudley Road, New Brunswick, New Jersey 08901, United States

[‡]State Key Laboratory of Polymer Physics and Chemistry, Changchun Institute of Applied Chemistry, Changchun 130022, P. R. China

Supporting Information

ABSTRACT: In protein−polysaccharide complex systems, how nonspecific interactions such as electrostatic and van der Waals interactions affect complex formation has not been clearly understood. On the basis of a coarse-grained model with the specificity of a target system, we have applied Monte Carlo (MC) simulation to illustrate the process of complex coacervate formation from the association of proteins and polysaccharides. The coarse-grained model is based on serum albumin and a polycation system, and the MC simulation of pH impact on complex coacervation has been carried out. We found that complex coacervates could form three ways, but the conventional association through electrostatic attraction between the protein and polysaccharide still dominated the complex coacervation in such systems. We also observed that the depletion potential always participated in protein crowding and was weakened in the presence of strong electrostatic interactions. Furthermore, we observed that the sizes of polysaccharide chains nonmonotonically increased with the number of bound proteins. Our approach provides a new way to understand the details during protein−polysaccharide complex coacervation at multiple length scales, from interaction and conformation to aggregation.

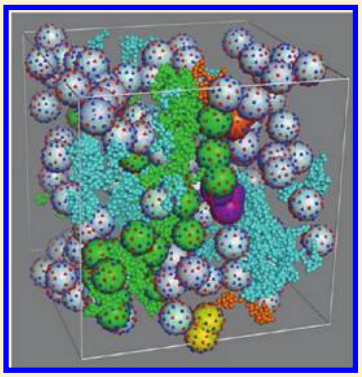

INTRODUCTION

Protein−polysaccharide complex coacervation is of great interest not only in scientific research but also in various biological and industrial applications. Complex coacervation is based on the ability of oppositely charged water-soluble polymers to associate through global phase separation to form a polymer-rich, dense liquid. Complex coacervates have been used in microencapsulation technology to produce a two-component ink system for carbonless copy paper.[1,2] More recently, the complex coacervates formed by proteins and polysaccharides have been used in protein separation and purification,[3,4] microencapsulation of food ingredients,[5] stabilization of emulsions for controlled release of free organic compounds,[6,7] enzymes,[8] cells,[9] pharmaceuticals,[10] and improving the in vitro anticancer activity of polyphenols,[11] etc. Considerable research has been exploited since the pioneering work of Tiebackx[12] and Bungenberg de Jong,[13] with the goal to present unequivocal descriptions of the physical nature and predictive rules for complex coacervation. A number of comprehensive reviews are available[14−19] for multiple aspects of complex coacervates. Unfortunately, protein−polysaccharide complex aggregates show strong dependency on multiple external factors (i.e., pH, temperature, and ionic strength, etc.) and intrinsic parameters (i.e., molecular weight, charge density, and charge distribution etc.), and widely applicable rules for the prediction of the phase behaviors in such complex systems still remain elusive.

In general, the composition, stability (or the association strength), structure, and their response to the change of external conditions are important characteristics in protein−polysaccharide complex coacervation. For external factors, the pH may be the most common factor to tune the properties and the structure of the complex coacervates formed by proteins and polysaccharides. For example, Espinosa-Andrews et al.[20] found that pH could strongly influence the microstructure and rheological properties of the aggregates of gum Arabic and chitosan. Weinbreck et al.[21] found that whey protein and gum Arabic have strong association at pH 4.0−4.2, and protein and polysaccharide diffused independently. Bohidar et al.[22] also reported that proteins diffused faster than polymers, and the dynamic property of complex coacervate was insensitive to the molecular weight of polyelectrolyte. Spruijt et al.[23] have reported typical binodal distribution of composition in coacervates as a function of salt concentration. At molecular scale, response to pH variation can be viewed by the change in intermolecular binding affinity and selectivity. Sanchez et al. reported that the rheological properties of whey−xanthan gum complex coacervates strongly depended on the self-aggregation of proteins when the pH was close to the isoelectric point (pI) of the whey protein, different from the protein−polysaccharide association when the pH was far from the pI of whey protein.[24] Dickinson[25] pointed out that the transition from a weak complex to a strong complex with pH variation depended on whether there were strong electrostatic interactions between the polysaccharide and protein. Overall, the pH dependence of protein−polysaccharide complex coacervates can be interpreted through electrostatic interaction, which can be

Received: July 10, 2011
Revised: January 23, 2012
Published: January 26, 2012

determined by the distribution of charges, a parameter closely related to the structure of the protein−polysaccharide complex coacervates.

The structure of the protein−polysaccharide complex coacervates typically has a gel network or a porous structure.[16,20,26] In some cases, the coacervates can be regarded as colloidal gels.[18,27] Thus, the coacervation may be considered as a geometrical percolation procedure similar to a sol−gel transition,[28−30] which can be investigated via computer simulations. In addition, a gel network can be classified as either a weak or a strong gel when the interaction energy is close to k_BT or far more than k_BT, respectively,[29] where k_B is the Boltzmann constant. For protein−polysaccharide complexes, when pH is at the "wrong side" of the pI of a protein,[31,32] the protein brings more charges of the same sign than that of the polyelectrolyte, and they normally form a weakly associated complex (e.g., soluble complex). On the other side, a protein brings charges of the opposite sign to the polyelectrolyte and strongly associates through electrostatic attraction. Thus, measuring the strength of intermolecular interactions can help address whether a complex is strongly or weakly associated. It provides a way to understand the relationship between the stability and rheological properties of the protein/polysaccharide complexes. Such knowledge on the correlation among intermolecular interactions, microstructures, and phase transition is of great interest for novel materials design at the molecular scale.

The other issue is how the molecular conformation changes during protein−polysaccharide complex formation and how the elementary interactions such as van der Waals interaction, electrostatic interaction, and entropy play roles during protein−polysaccharide complex formation. It has been reported that entropy-dominated systems have typically collapsed microstructures and polymer chains,[33] whereas in enthalpy-dominated systems, polymer chains can enwrap on the surface of large colloids.[34,35] A number of simulation papers related to the complex formation through either interaction with a single protein,[35] a single polysaccharide chain,[35−37] or at a pH around the pK_a of the polysaccharide or the pI of the protein[35,38,39] have been published. However, a simulation work that takes into account the multibody effect similar to the entropy-dominated systems and the specificity of interactions may provide new insights into protein−polysaccharide complexes.

In this work, we use Monte Carlo simulation to study the complex and complex coacervation in a protein−polysaccharide system. A coarse-grained model based on the characteristic charge distribution of serum albumin and a polycation was set up first. Simulations guided by nonspecific interactions were subsequently carried out, and the intermolecular interactions were analyzed. Three pathways to form protein−polysaccharide complexes were then observed, and their contributions to coacervation were studied. The size distribution of the complex aggregate and the microstructure in the system were investigated using pair correlation function and percolation concepts, and the conformation distribution of polysaccharide chains was analyzed. Finally, we elucidated the simulation results at multiple length scales, from intermolecular interaction and polymer conformation to complex association.

METHODS

In this work, we use serum albumin and a polycation as the actual reference systems to setup simulation model. A schematic diagram for the simulation model is illustrated in Figure 1, in which the protein (PRO) was modeled as a soft sphere with charge patches on its surface, and the polysaccharide (PS) was modeled as a freely jointed chain with soft beads. Each charge patch and soft bead carries partial charges under different pH values following dissociation equilibrium.

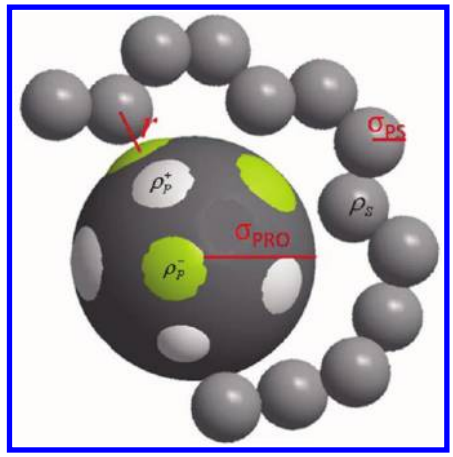

Figure 1. Schematic of the simulation models. The spheres of proteins and polysaccharide (PS) segments have a radius of σ_{PRO} and σ_{PS}, respectively. Charge patches in the protein surface bring partial charges of ρ_P^+ and ρ_P^-, and each PS segment brings a partial charge of ρ_S. The distance r is used to calculate the electrostatic interaction between a PS segment and a charge patch.

Modeling of Protein and Polysaccharide. Proteins were considered as soft spheres with charge patches on their surfaces. The equivalent gyration radius of the sphere is 30 Å,[40] which is close to the gyration radius of all atoms except hydrogen atoms, on the basis of the native structure of human serum albumin (HSA, PDB id: 1e7i). The gyration radius is 28.4 Å using the method described in our recent work.[41]

In all the 585 residues of HSA, 99 potential residues are positively charged (R, K, and H) and 115 potential residues are negatively charged (D, E, and Y). When the pH is lower than the pK_a of an isolated amino acid, protonation in the side-chain group results in a positively charged residue (R, K, and H), whereas a negatively charged residue (D, E, and Y) is formed when the pH is higher than the pK_a of dissociation. In consideration of the exposed residues assigned using DSSP,[42] the 70 positively charged residues and 91 negatively charged residues (i.e., titratable residues[43]) can be assembled into continuous patches when the β-carbons in any two residues approach to less than 12 Å. The number of charge patches and the total positive/negative charges held in charge patches were calculated according to basic−acidic equilibrium and are shown in Table 1. It is worth noting that the conventional definition of charge patch is based on the Poisson−Boltzmann continuum electrostatic potential around a protein, calculated using DelPhi[44,45] or UHBD[46,47] etc. Here, we propose a simple and direct definition of protein charge patches, which are structural motifs composed of a cluster of residues with the same sign of charges and are potentially accessible by other molecules to form strong binding.

Each polysaccharide molecule was modeled as a freely jointed chain (FJC) with soft beads connected at fixed bond lengths. Each bead with a radius of 5.0 Å corresponds to a disaccharide unit,[48,49] which brings a partial charge at the center of mass. The ultimate protonation of the bead brings one unit charge when the pH is much lower than the pK_a of the cationic group.

dx.doi.org/10.1021/jp206527p | J. Phys. Chem. B 2012, 116, 3045−3053

Table 1. Dependence of Charge Distribution on pH in Protein and Polysaccharide (PS) Chain[a]

particles		charges for each particle							
	pH	3.5	4.0	5.0	6.0	7.0	8.0	10.5	12.0
protein	r_+	48.4/27	41.7/25	28.3/27	18.5/27	3.3/24	1.3/24	0.03/9	0/0
	r_-	0/0	−31.0/23	−85.0/30	−85.0/30	−85.0/30	−85.0/30	−91.0/28	−91.0/28
PS		0.99	0.98	0.96	0.90	0.76	0.53	0.08	0

[a]A pK_a value of 6.7 was taken for the PS chain. For the protein, the total positive charges/the number of positively charge patches (r_+) and the total negative charges/the number of negatively charge patches (r_-) were presented at each pH.

Charge Distribution. For the dissociation equilibrium of a weak electrolyte, that is, HA ⇌ H^+ + A^-, the fraction of the charged group has the relationship of $[A^-]/[HA] = 10^{pH-pK_a}$, where K_a is the dissociation constant. Assuming that each dissociable/associable group brings a unit charge, at a given pH, the negatively charged group (e.g., $-COO^-$) brings a partial charge of $(10^{pH-pK_a}/(1 + 10^{pH-pK_a}))$, and the positively charged group (e.g., $-NH_3^+$) brings a partial charge of $10^{pK_w-pH-pK_a}/(1 + 10^{pK_w-pH-pK_a})$, with pK_w (equal to 14) being the equilibrium constant of pure water at ambient temperature. According to the pK_a values of isolated amino acids (R 12.0, K 10.5, H 6.08, D 3.9, E 4.3, and Y 10.1), the sum of charges from all the charged residues in each patch could be obtained. The charge patches were grouped into positively charged patches and negatively charged patches. The detailed information of charge patches changed with the pH can be found in Table S1 in the Supporting Information. Similarly, the partial charge of polysaccharide segment was calculated by using the pK_a of 6.7. Then the charge patches of each protein were randomly distributed on the protein surface with a mutual spatial separation of no less than 12 Å. Each patch has a partial charge according to the basic−acidic equilibrium at each pH value. The amount of partial charges in the polycation segment is also determined by the protonation of $-NH_2$ at each pH value and located at the center of each segment.

Interactions. Two nonspecific elementary interactions, van der Waals interaction and electrostatic interaction, were considered in the simulation system. The total potential energy in the system is

$$U = \sum_{i,j} [U_{EV}(i, j) + U_{ELE}(i, j)] \quad (1)$$

The excluded-volume (EV) potential is calculated from the summation of the Lennard-Jones potential through

$$U_{EV}(i, j) = \varepsilon_{ij}\left[\left(\frac{\sigma_{ij}}{r_{ij}}\right)^{12} - 2\left(\frac{\sigma_{ij}}{r_{ij}}\right)^{6}\right] \quad (2)$$

where $\sigma_{ij} = (\sigma_i + \sigma_j)/2$ and $\varepsilon_{ij} = (\varepsilon_i\varepsilon_j)^{1/2}$ with σ_i and ε_i (fixed at $1.0k_BT$ in this work) are the van der Waals radii and the potential well of polysaccharide segment and protein, respectively. The electrostatic potential was calculated through Debye−Hückle approximation, that is,

$$U_{ELE}(i, j) = \frac{q_i q_j}{4\pi\varepsilon_0\varepsilon_r r_{ij}} \exp\left(-r_{ij}/\lambda_D\right) \quad (3)$$

where q_i, q_j are the partial charges of each charged patch on the protein surface and the PS segment; ε_0 is the vacuum permittivity; ε_r is the relative dielectric permittivity constant; and λ_D is the screening length fixed at 10.0 Å, which corresponds to 0.1 mol/L monovalent salt solution. The constant $(4\pi\varepsilon_0\varepsilon_r)^{-1}$ is set as 2.0 $(k_BT\text{Å}/e^2)$ with e being the charge unit. To define whether two molecules are bound together, the intermolecular interaction, U, which is the sum of all interaction pairs between two molecules according to eq 1, was calculated and compared with $-\Gamma k_BT$, where Γ is a positive constant that controls the strength of holding an aggregate. When U is stronger than $-\Gamma k_BT$, the two molecules are regarded as associated.

Table 2. Parameter Settings in the Monte Carlo Simulation

simulation box length	48 nm
radius of protein (σ_{PRO})	3.0 nm
radius of PS segment (σ_{PS})	5.0 Å
no. of proteins	140
no. of PS chains	30
no. of segments in each PS chain	200
volume fraction of proteins	0.143
volume fraction of PS chains	0.028
screening length, λ_D	10.0 Å

Simulation Settings. In Table 2 we present the parameter settings in the Monte Carlo simulation. The solvent was implicitly modeled as a dielectric continuum. The simulation is guided under Metropolis rule.[50] For conformation sampling, each polysaccharide chain was subjected to translational trial moves of (i) the crank rotation of the in-between segments around the axis through the two head segments by random selection, at a random angle in [−180°, 180°]; (ii) the pivot rotation of one end of the chain around an arbitrary axis passing through the conjoined segment with a random angle; and (iii) a slithering move at either end of the whole chain. All these movements on the polysaccharide chains did not change the bond length between two connected segments. Two movements were used to diffuse proteins: one is the transition of a whole protein along a random vector, and the other is the spin of a protein around a random axis passing its center. To accelerate the calculation of electrostatic potential, a truncation of 18 Å[51] was adopted.

Proteins and polysaccharides (PS) were evenly distributed in a cubic simulation box under periodic boundary conditions in every direction before simulation. A Monte Carlo simulation with 2×10^5 MCS relaxation guided by U_{EV} was used only to eliminate artificial impact on the initial configurations. Here, the MCS represents a Monte Carlo step, the time scale for each PS segment or protein to have one attempt of movement. Then all energy terms were turned on, and a simulation of 1.8×10^6 MCS was carried out to achieve thermodynamic equilibrium. Four parallel trajectories at each point were simulated, and the last 25 out of 200 configurations from each trajectory were extracted and analyzed. Therefore, in the following part, without special mention, all the results are from the average of 100 configurations under thermodynamic equilibrium.

dx.doi.org/10.1021/jp206527p | J. Phys. Chem. B 2012, 116, 3045−3053

To illustrate how proteins and polysaccharides are mutually affected in aggregation, two sets of control simulations were also carried out. In the control simulation, the system contains only either PS chains or proteins. The volume fractions and interactions of PS and protein are the same as those in the mixture systems, and the simulations were collected in the same way as described above.

Complex and Complex Coacervation. A protein−polysaccharide complex is formed when their intermolecular interaction has attractive potential stronger than $\Gamma k_B T$. The larger the absolute value of Γ, the stronger the intermolecular binding affinity. In fact, because one PS chain may be adsorbed to multiple charge patches on protein surfaces, or one protein may bind to multiple PS chains through different binding sites, cross-linking between them results in the classical complex coacervation model first described by de Joon.[52] Therefore, a complex can be defined as an aggregate containing at least one PS chain and one protein. A complex can further aggregate to form a coacervate or percolated network through the bridging effect by PS chains and proteins. Since either PS or protein carries many binding sites, the complex can expand quickly, and the largest aggregated domain (coacervate) may hold all PS chains and proteins.

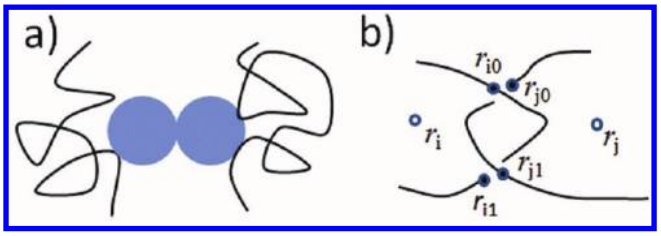

Figure 2. Schematic diagram of two ways for complex coacervation: (a) through protein self-aggregation, and (b) through entanglement of polysaccharide chains.

In reality, in addition to the classical association between proteins and PS chains, two other types of intermolecular aggregation may also contribute to protein−polysaccharide complex coacervation. One is that a complex can be expanded through self-aggregation of proteins when two proteins have an attractive interaction stronger than $\Gamma k_B T$ (Figure 2a). The other is that the entanglement of PS chains can also enlarge a complex (Figure 2b). To identify an entanglement knot, at least two "cross-linked" pairs are required. The pair is formed from two segments of nonidentical chains with their distance less than $R_{entangle}$, which equals the sum of the van der Waals radii of the segment and the smallest space to allow a minimum particle in the system to pass through them, that is, $4\sigma_{PS}$ in this work. On the basis of Figure 2b, a morphological definition of entanglement between chain i and chain j satisfies the following criteria:

$$\left|r_{i0} - r_{j0}\right| < R_{entangle} \quad \text{and} \quad \left|r_{i1} - r_{j1}\right| < R_{entangle} \tag{4a}$$

$$(r_i - r_j)\bullet(r_{i0,i1} - r_{j0,j1}) \leq 0 \tag{4b}$$

$$(r_{i0} - r_{j0})\bullet(r_{i1} - r_{j1}) \leq 0 \tag{4c}$$

where r_{i0}, r_{j0}, r_{i1}, and r_{j1} are the positions of segment $i0$, $j0$, $i1$, and $j1$, respectively; r_i and r_j are the positions of the center of mass of chain i and chain j, respectively; and $r_{i0,i1}$ and $r_{j0,j1}$ are the positions of the center of mass of the segments between segments $i0$ and $i1$, $j0$ and $j1$, respectively. In the Results section, we consider three kinds of aggregates: (1) pure protein−PS association (type I aggregate); (2) type I plus protein self-aggregation (type II aggregate), and (3) type II plus PS entanglement (type III aggregate).

RESULTS

Distribution of Intermolecular Interactions and Aggregations. The distribution of intermolecular interactions is shown in Figure 3. It can be seen that for PS−PRO interactions, <10% are negative when pH < 5.0. Under this situation, PS segments are positively charged, and the net charge of the protein is also positive. The strong electrostatic repulsion between the PS segment and the positive charge patches in the proteins leads to the repulsive intermolecular interactions. At pH values ranging from 5.0 to 7.0, around 40% of PS−PRO pairs are negatively charged, and the attractive strength increases as the pH is increased. When the pH is higher than 7.0, the number of PS−PRO attractive pairs decreases with an increase in the pH as a result of weakening of the electrostatic attraction due to the drastic decrease of positive charges brought by PS segments.

For protein−protein interactions, around 40% of pairs are positive (repulsive). The energy penalty from the overlap of the excluded volume of proteins is majorly compensated from the entropy gain of small PS segments, known as a consequence due to the depletion effect.[53] Electrostatic attraction may also contribute to the close packing of proteins, but it has no

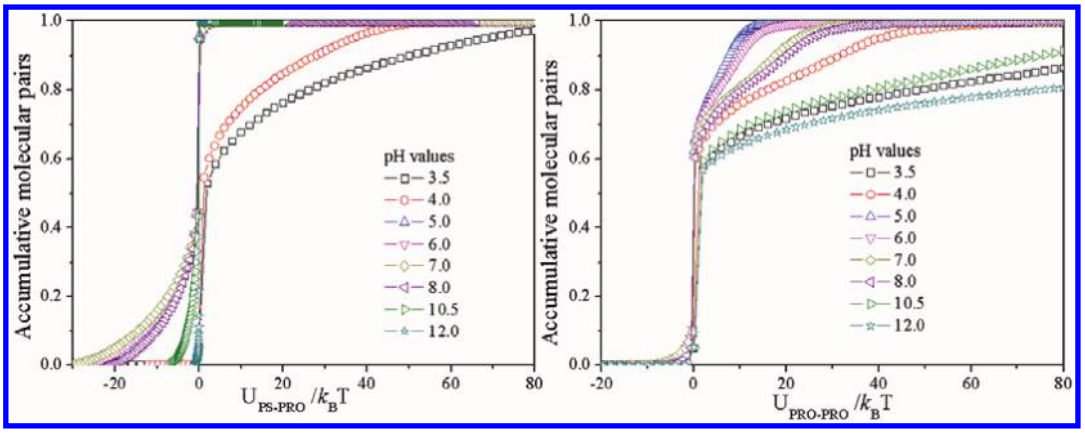

Figure 3. Distribution of intermolecular interactions under different pH values.

dx.doi.org/10.1021/jp206527p | J. Phys. Chem. B 2012, 116, 3045−3053

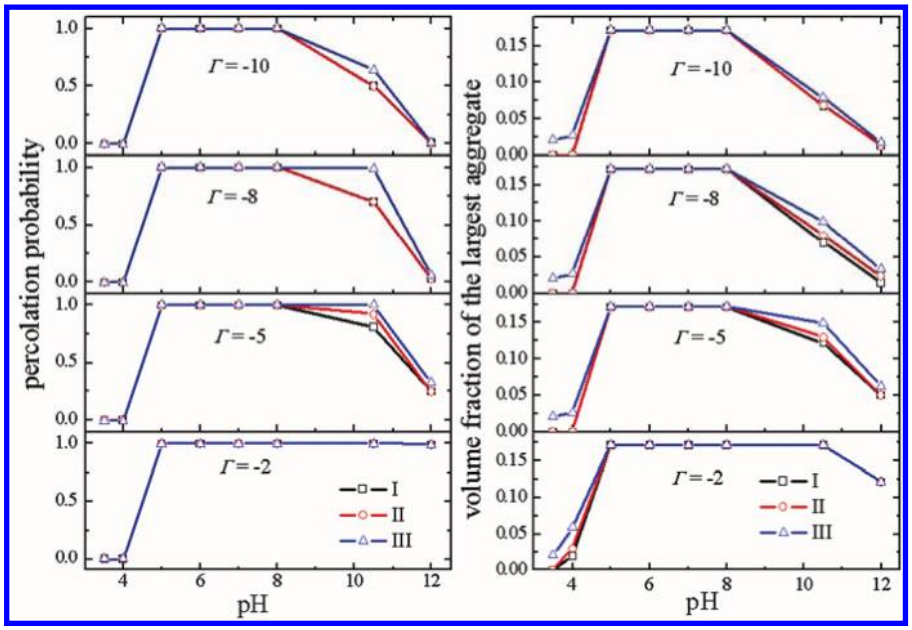

Figure 4. The effects of pH on percolation probability (left) and the volume fraction of the largest aggregate (right) at different intermolecular interaction cutoffs. Black squarse, red spheres, and blue triangle represents aggregates of type I, II, and III respectively.

remarkable favor for the overlap of excluded volume of proteins. Through comparison of the charge distributions at pH 5.0 and 12.0, proteins were found to have the least overlap at pH 5.0, and the highest degree of excluded volume overlap and the largest energy penalty occurred at pH 12.0, where the energy penalty was exclusively compensated by the strongest depletion force in the presence of neutral PS segments. It suggests that the presence of electrostatic interaction can weaken the depletion effect. Similarly, it can also be found that the neutral polymer−colloid system has a stronger depletion force than that in charged polymer−colloid systems from a comparison of the distribution of intermolecular interactions at pH 3.5 and 12.0.

As mentioned above, whether a molecule belongs to the aggregate of a complex or complex coacervate domain is determined by the molecule whose intermolecular interaction with any molecule in the aggregate is stronger than $\Gamma k_B T$. Then the aggregates can be identified according to different Γ values through three different manners, named as types I, II, and III. Furthermore, we regarded the aggregate that geometrically percolated the simulation box as a complex coacervate domain, and the sample (simulation configuration under thermodynamic equilibrium) was considered as percolated. We then calculated the probability of percolation, the same as that used in our previous work[54] to define the percentage of percolated samples.

We also calculated the volume fraction of the largest aggregate in the simulation systems and then plotted them against pH (Figure 4). These three types of aggregates had different percolation probabilities when the threshold was set for strong intermolecular association. When the threshold Γ was set to −2, which corresponds to weak intermolecular association, the classical complex manner (type I) dominated the complex formation. When Γ was set to an intermediate value, the strong electrostatic attraction between PS−PRO dominated complex formation at low pH values. However, at the high pH region, the electrostatic interaction between the PS and protein became weak, and protein self-aggregation and PS entanglement showed visible contribution to the complex formation. When Γ was −10, a threshold for very strong intermolecular association, protein self-aggregation was negligible, but the entanglement of the PS chain still made a visible contribution at low and high pH values.

For the distribution of the largest aggregates at pH 3.5 and 4.0, the protein and PS chain have a strong electrostatic repulsion, and aggregation through PS−PRO association and protein self-aggregation become almost impossible; only the aggregates through entanglement of PS chains can be observed. At pH 12.0, van der Waals attraction between a protein and neutral PS chain and entanglement become the major contribution to sustaining the complex. In the whole pH range, a small fraction of the PS chains are always entangled, although they may not be visible when the pH is in the vicinity of the pI.

Since the percolation probability profile can be used to determine phase boundaries,[30,55−57] the pH dependence of the percolation probability here is comparable with the turbidity titration curve. By comparing our results with the pH-dependent turbidimetric titration curve from a BSA−chitosan system,[58] we found that the phase diagram using the threshold of strong intermolecular association from our simulation is very close to the experimental observations. This result suggests that the complex of a BSA−chitosan system is stabilized by a strong intermolecular binding affinity.

Snapshots of Simulation. After the identification of three types of aggregates, an illustration of the configuration under thermodynamic equilibrium from the Monte Carlo simulation was presented in Figure 5. It can be clearly seen that the association of PS chains and proteins through strong attractive interactions is the main mechanism for complex formation (type I). Protein self-aggregation can further promote the complex coacervation through electrostatic attraction among oppositely charged patches in the proximity of protein surfaces (type II). Then the entanglement of polysaccharide (PS) chains with their bound proteins can further expand the complex coacervate (type III). We also observed that two proteins were suppressed with highly overlapped excluded volume. The strong steric repulsion (van der Waals interaction) between

dx.doi.org/10.1021/jp206527p | J. Phys. Chem. B 2012, 116, 3045−3053

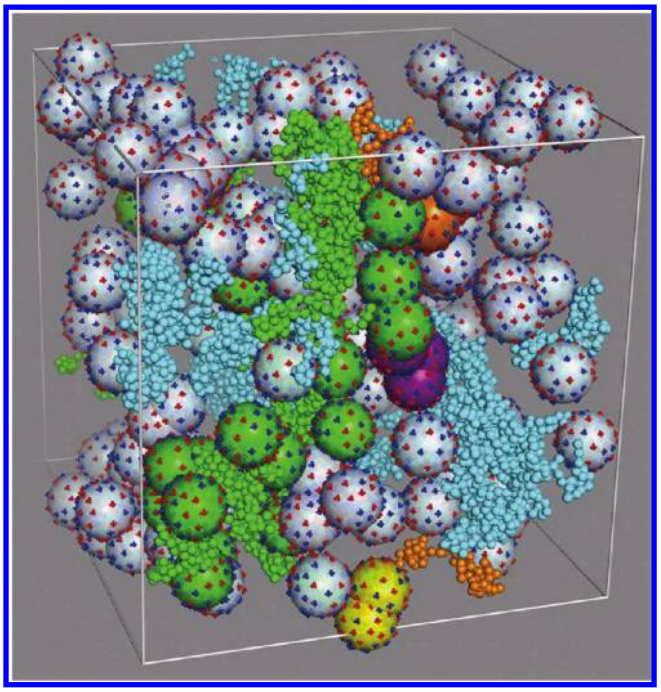

Figure 5. Snapshot of the simulation configuration (pH 10.5). The cyan strings of beads are polysaccharide (PS) chains, and the large isolated spheres are proteins. The red dots and blue dots on the protein surfaces are positive and negative charge patches, respectively. The green indicates the type I aggregate (classical complex) formed through strong intermolecular interactions (PS−PRO attractive interaction stronger than $-8k_BT$). The purple-colored complex expanded through protein self-aggregation ($<-8k_BT$ attraction, type II aggregate), and the orange-labeled aggregate is further enlarged through entanglement of PS chains (type III aggregate). The depletion-induced protein aggregation can also be observed at the bottom, where two proteins are highly overlapped (yellow).

them can be overwhelmed through the depletion force from the spatial competition between PS segments and proteins.

Microstructure of the Protein/Polysaccharide Complex. We characterized the microstructure in the protein/polysaccharide complex using a pair correlation function (PCF), which is defined as

$$g(r)_{XY} = \frac{\sum_i \sum_j \delta\left(r - \left|\vec{r}_{X,i} - \vec{r}_{Y,j}\right|\right)}{4\pi r^2 C_{XY}} \quad (5)$$

In this formula, X and Y are PS segments or proteins, C_{XY} is a constant used to normalize long-range correlation to unit value. $\delta(t)$ is the delta function, which equals 1 if t equals 0 (otherwise, it is zero), and $\vec{r}_{x,i}$ is the location of the ith X particle (either a PS segment or a protein). The PCFs of PS−PS, PRO−PRO, and PS−PRO are shown Figure 6. The strength of the PCF corresponds to the aggregation of two particles, with a value larger than 1 denoting extra aggregation above an even distribution and values less than 1 indicating a depletion of particles. In the calculation of the PCF of PS−PS, we count only segment pairs from different chains.

The PCF profiles of PS−PS show weak aggregation from pH 3.5 to 5.0, where the PS segment brings strong positive charges and electrostatic repulsion inhabits the aggregation of PS segments at a large scale. From pH 5.0 to pH 8.0, the interchain

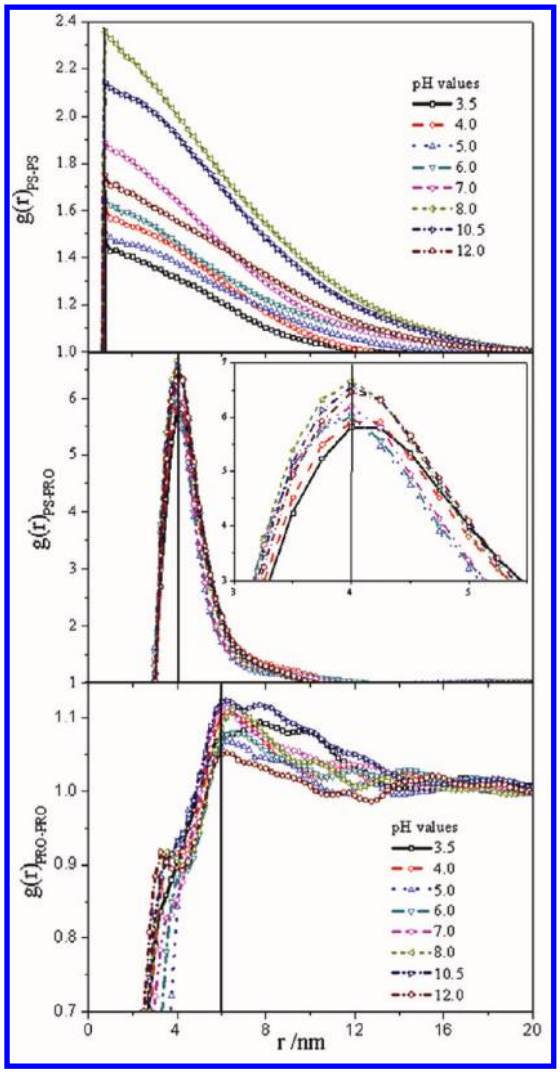

Figure 6. Correlation functions of polysaccharide (PS) segments and proteins. The vertical solid line shows the location of the van der Waals potential well between two particles.

aggregation strengthened as the number of charges decreased, and from pH 8.0 to 12.0, the interchain aggregation decreased as a result of the association of PS and proteins competing with the PS interchain aggregation. This can be found through a comparison of the results from the control simulation (see Supporting Information Figure S1), where the PCF of PS−PS monotonically increased as the pH increased. Further comparison of PCFs indicates that the extra aggregation of interchain PS segments within a short separation distance was remarkably enhanced in the presence of proteins.

On the basis of the PRO−PRO PCF profiles, the protein intermolecular aggregation has been enriched in the separation distance from 6.0 to 13.0 nm. The depletion layer due to the excluded volume of proteins could be seen when proteins separated less than 6.0 nm, and it is sensitive to pH. According to the least separation distance among proteins, proteins are less suppressed at medium pH values, that is, pH 5.0, 6.0, and 7.0, whereas at pH 12.0, proteins are the most suppressed. Compared with the PCF of PRO−PRO from the control simulation (see Supporting Information Figure S1), the enrichment of protein packing in the depletion layer can be clearly seen. It may be contributed from two aspects: one is that

dx.doi.org/10.1021/jp206527p | J. Phys. Chem. B 2012, 116, 3045−3053

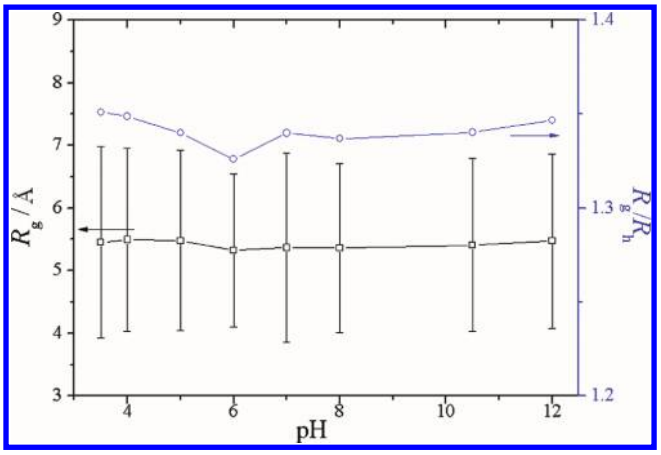

Figure 7. The radius of gyration (R_g) and the R_g/R_h ratio of polysaccharide (PS) chains change with pH.

the complex formation between the PS chain and proteins leads to local enrichment of proteins; the other is that the spatial competition between proteins and PS segments deriving from depletion force always promotes extra aggregation of proteins.

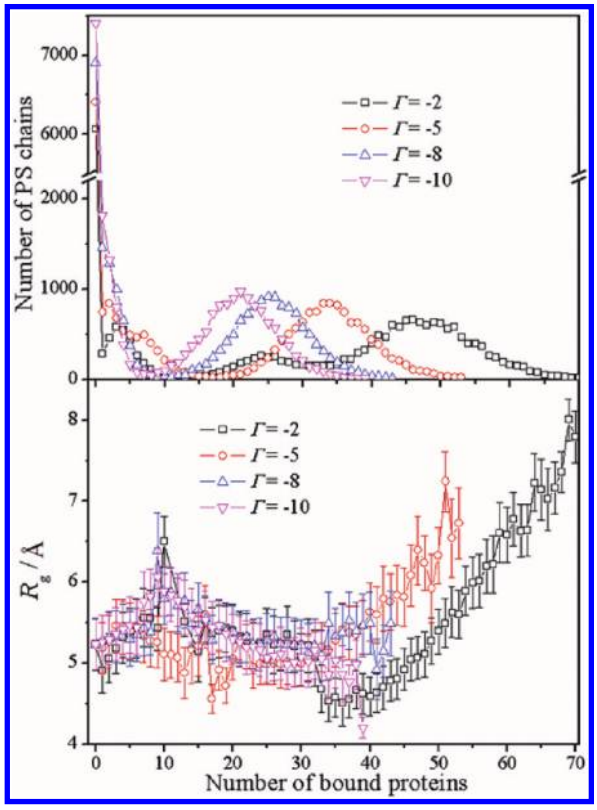

Figure 8. The number of polysaccharide (PS) chains (upper panel) and the average size of the PS chains (bottom panel) distributed against the number of bound proteins on each PS chain at different thresholds of intermolecular interactions.

On the basis of the PS–PRO PCF profiles, the aggregation between PS segments and proteins increased when the pH increased from 3.5 to 8.0, and the aggregation decreased with a further increase in the pH. Electrostatic attraction is the major contributor for the aggregation of PS segments and proteins. At a low pH range, a higher pH value corresponds to more negatively charged patches in the proteins, which promotes the association with positively charged PS segments, whereas at a high pH range, the weak positive charges in the PS segment diminish quickly along with the electrostatic attraction between the PS segment and protein, resulting in less PS–PRO aggregation due to the balance of conformation entropy loss and van der Waals interaction.

Conformation of Polysaccharide Chains. The average radius of gyration (R_g) of PS chains and the ratio between R_g and the hydrodynamic radius (R_h) to characterize the sizes and shapes of PS chains are plotted against pH in Figure 7. It can be seen that both the sizes and shapes of the PS chains are almost independent of the pH. The average of R_g at different pH values is around 5.4, which is slightly smaller than that from the control simulation (5.7, see Figure S2 in the Supporting Information). This result indicates that the addition of proteins slightly leads to the collapse of PS chains, which is consistent with previous reports that show that the presence of protein could induce collapse of polymer chains.[59] The ratio of R_g/R_h is around 1.34 (1.36 from control simulation), which suggests that the PS chains should be random coils in a θ-solvent.[60,61]

We further studied the dependence of R_g on the number of bound proteins under different thresholds of intermolecular interactions, and the results are shown in Figure 8. The distribution of PS chains shifted to less-bound proteins upon an increase in the threshold. The size of the PS chains showed nonmonotonic dependence upon the number of bound proteins. It first increased with the bound proteins when the number of bound proteins was less than 10 per chain, then decreased with a further increase in the bound proteins until it reached around 35 bound proteins per chain, followed by the size increase with more bound proteins. The size had a weak dependence on the threshold when few proteins are bound, but is significantly different when more proteins are bound. For a PS chain with the same number of bound proteins, PS chains with stronger binding affinity were relatively larger in size.

DISCUSSION

We have observed the contribution of polysaccharide (PS) chains' entanglement to complex formation of PS and proteins based on a morphological definition in the simulation. One may question whether the PS chains can entangle with each other. This involves whether the PS chains exceeded the critical entanglement length in units of Kuhn segments. The critical entanglement length is around 30 Kuhn units[62] according to the previous report. On the basis of our simulation, the number of Kuhn segments of PS chains, N_K, calculated through $N_K = L^2/6R_g^2$ using the model by Tuinier[63] is around 227 or 50 calculated through $N_K = LC/(C+1)^2$ with $C = 6R_g^2/Nb^2$ using the method by Wang.[64] In the latter formula, $L = Nb$ is the contour length of a PS chain with N segments, and each segment has a size of b. Both results indicate that PS chains in our simulation system can entangle mutually.

Proteins can self-aggregate through van der Waals attraction and electrostatic attraction among oppositely charge patches. The self-aggregation has significant impact on the microstructure of coacervate, which has been reported in β-lactoglobulin/pectin mixtures.[65] However, in this simulation work, under a given threshold of intermolecular interaction, we found that protein self-aggregation played a less important role, either to increase percolation probability or to enwrap more molecules in the largest aggregate. It can also be viewed in Figure S1 of the Supporting Information that no percolated

dx.doi.org/10.1021/jp206527p | J. Phys. Chem. B 2012, 116, 3045–3053

simulation configuration was found in the control simulation of pure proteins, which is directly originated from weak protein−protein attractive interactions (large excluded volume and competition of electrostatic attraction and repulsion among charge patches). It suggests that the difference in self-aggregation propensity between BSA and β-lactoglobulin may stem from the difference in the specific distribution of charge patches in their native structures. Careful tuning of the distribution of charge patches is critical to observe the contribution of protein self-aggregation in protein−polysaccharide complex coacervation. For example, Jonsson et al. found that polymer adsorption was promoted for proteins with more heterogeneous (clustered) site distributions, as opposed to more homogeneous distributions of the hydrophobic sites.[66] Further investigation on how the self-aggregation of proteins affects the microstructure of a complex coacervate is undergoing.

Conventionally, a protein−polysaccharide system is treated as a colloid−polymer mixture. An abundance of research papers have been published to emphasize the contribution of entropy or the well-known depletion effect.[67] An exhaustive review on how proteins and PSs of different sizes affect the aggregation and microstructure can be found here.[33] Through comparison of the PCF of PRO−PRO from the simulation with that from the control simulation, extra aggregation of proteins in the presence of PS chains can be clearly observed. Verma et al. found that in a polymer−colloid system, the strongest depletion occurred when the polymer coils and the colloid were of comparable sizes.[68] In our study, the diameter of proteins and the R_g of PS chains are very close. It is not surprising if they have a strong depletion force, and the strongest depletion force occurs when PS chains are neutral. The presence of electrostatic interaction (both attractive and repulsive) weakened the depletion effect, resulting in less crowding of proteins. This result is different from the observation in a weakly charged colloid and neutral polymer system, in which the increase in the electrostatic repulsion among colloids inhibited demixing,[69] or the recent observation by Buzzaccaro et al. that the screening of electrostatic repulsion would lead to less aggregation of colloid.[70] The bifurcation here suggests that we need to be careful when trying to migrate the results from colloid−polymer systems to support the observations in protein−polysaccharide systems, as previously pointed out by Doublier et al.[15] More investigations are still underway to understand how the electrostatic interaction weakens the depletion effect in the protein−polysaccharide systems.

On the other hand, current modeling still has a lot of room to improve to present more realistic information in protein−polysaccharide complex coacervation. For example, HSA is not completely spherical, since it has a long to short axial ratio of 2 to 4 and is sensitive to pH.[71,72] Charge patches are not randomly dispersed on a protein surface, but specially orientated referring to the center of the protein. The charge density in a polysaccharide chain should affect the stiffness,[73,74] which further has influence on the distribution of the conformation of polysaccharide chains. Our current model of polysaccharide chains using a free rotation chain model has not fully expressed such a trend. Further research concerning nonspherical and specialized distribution of charge patches on the protein surface and charge induced persistence length in polysaccharide chains are still underway.

CONCLUSION

In this work, we carried out Monte Carlo simulation to study complex formation in globular protein (e.g., bovine serum albumin and β-lactoglobulin) and cationic polysaccharide mixtures. The effect of pH on the distribution of charges, the complex coacervation coupling with intermolecular associations, and the microstructure of complex coacervate were investigated. We found that the self-aggregation of proteins and the entanglement of polysaccharide chains play a remarkable role in complex coacervation, which is complementary to conventional understanding of protein−polysaccharide complex coacervation. We also observed that the depletion potential always participated in the stabilization of complex coacervate, especially for the crowding of proteins. The presence of electrostatic interactions can significantly weaken the depletion force. Although current modeling is still naive, this work nevertheless provided abundant meaningful information for the better understanding of protein−polysaccharide complexes and complex coacervation.

ASSOCIATED CONTENT

Supporting Information

Simulation results from control simulations and the details of distribution of charge patches in coarse-grained protein models. This material is available free of charge via the Internet at http://pubs.acs.org.

AUTHOR INFORMATION

Corresponding Author

*(Q.H.) Phone: 732-932-7193. Fax: 732-932-6776. E-mail: qhuang@aesop.rutgers.edu. (L.A.) Phone: +86-431-5262296. Fax: +86-431-5685653. E-mail: ljan@ciac.jl.cn.

Author Contributions

§These authors contributed equally.

Notes

The authors declare no competing financial interest.

ACKNOWLEDGMENTS

This work was supported by United States Department of Agriculture National Research Initiative (No. 2009-35603-05071, QH) and in part by the National Natural Science Foundation of China (51028301, QH) and the Fund for Creative Research Groups (50921062, T.S. and L.A.).

REFERENCES

(1) Green, B. K.; Schleicher, L. U.S. Patent Application 2 730 456, *The National Cash Register*, 1956.
(2) Green, B. K.; Schleicher, L. U.S. Patent Application 2 800 457, *The National Cash Register*, 1957.
(3) Bedie, G. K.; Turgeon, S. L.; Makhlouf, J. *Food Hydrocolloids* **2008**, *22*, 836.
(4) Xu, Y.; Mazzawi, M.; Chen, K.; Sun, L.; Dubin, P. L. *Biomacromolecules* **2011**, *12*, 1512.
(5) Dziezak, J. D. *Food Technol.* **1988**, *4*, 136.
(6) Liu, S.; Low, N. H.; Nickerson, M. T. *J. Am. Oil Chem. Soc.* **2010**, *87*, 809.
(7) Renard, D.; Robert, P.; Lavenant, L.; Melcion, D.; Popineau, Y.; Gueguen, J.; Duclairoir, C.; Nakache, E.; Sanchez, C.; Schmitt, C. *Int. J. Pharm.* **2002**, *242*, 163.
(8) Singh, O. N.; Burgess, D. J. *Pharm. Sci.* **1996**, *2*, 223.
(9) Gibbs, B. F.; Kermasha, S.; Alli, I.; Mulligan, C. N. *Int. J. Food Sci. Nutr.* **1999**, *50*, 213.
(10) Kayes, J. B. *J. Pharm. Pharmacol.* **1977**, *29*, 163.
(11) Ru, Q. M.; Yu, H. L.; Huang, Q. R. *J. Agric. Food Chem.* **2010**, *58*, 10373.
(12) Tiebackx, F. W. Z. *Chem. Ind. Kolloide* **1911**, *8*, 198.

(13) Bungenberg de Jong, H. G.; Kruyt, H. R. *Proc. K. Ned. Akad. Wet.* **1929**, *32*, 849.
(14) de Kruif, C. G.; Weinbreck, F.; de Vries, R. *Curr. Opin. Colloid Interface Sci.* **2004**, *9*, 340.
(15) Doublier, J. L.; Garnier, C.; Renard, D.; Sanchez, C. *Curr. Opin. Colloid Interface Sci.* **2000**, *5*, 202.
(16) Schmitt, C.; Sanchez, C.; Desobry-Banon, S.; Hardy, J. *Crit. Rev. Food Sci. Nutr.* **1998**, *38*, 689.
(17) Turgeon, S. L.; Beaulieu, M.; Schmitt, C.; Sanchez, C. *Curr. Opin. Colloid Interface Sci.* **2003**, *8*, 401.
(18) Veis, A. *Adv. Colloid Interface Sci.* **2011**, *167*, 2.
(19) Gucht, J. v. d.; Spruijt, E.; Lemmers, M.; Cohen Stuart, M. A. *J. Colloid Interface Sci.* **2011**, *361*, 407.
(20) Espinosa-Andrews, H.; Sandoval-Castilla, O.; Vazquez-Torres, H.; Vernon-Carter, E. J.; Lobato-Calleros, C. *Carbohydr. Polym.* **2010**, *79*, 541.
(21) Weinbreck, F.; Rollema, H. S.; Tromp, R. H.; de Kruif, C. G. *Langmuir* **2004**, *20*, 6389.
(22) Bohidar, H.; Dubin, P. L.; Majhi, P. R.; Tribet, C.; Jaeger, W. *Biomacromolecules* **2005**, *6*, 1573.
(23) Spruijt, E.; Westphal, A. H.; Borst, J. W.; Cohen Stuart, M. A.; van der Gucht, J. *Macromolecules* **2010**, *43*, 6476.
(24) Sanchez, C.; Schmitt, C.; Babak, V. G.; Hardy, J. *Nahrung-Food* **1997**, *41*, 336.
(25) Dickinson, E. *Soft Matter* **2008**, *4*, 932.
(26) Mezzenga, R.; Schurtenberger, P.; Burbidge, A.; Michel, M. *Nat. Mater.* **2005**, *4*, 728.
(27) Burgess, D. J.; Singh, O. N. *J. Pharm. Pharmacol.* **1993**, *45*, 586.
(28) Stauffer, D.; Aharony, A. *Introduction to Percolation Theory*, 2nd ed.; Taylor & Francis: 2003.
(29) Kumar, S. K.; Douglas, J. F. *Phys. Rev. Lett.* **2001**, *87*, 188301.
(30) Li, Y.; Sun, Z.; Shi, T.; An, L. *J. Chem. Phys.* **2004**, *121*, 1133.
(31) Biesheuvel, P. M.; Cohen Stuart, M. A. *Langmuir* **2004**, *20*, 2785.
(32) de Vries, R.; Weinbreck, F.; de Kruif, C. G. *J. Chem. Phys.* **2003**, *118*, 4649.
(33) Fuchs, M.; Schweizer, K. S. *J. Phys.: Condens. Matter* **2002**, *14*, R239.
(34) Cooper, C. L.; Dubin, P. L.; Kayitmazer, A. B.; Turksen, S. *Curr. Opin. Colloid Interface Sci.* **2005**, *10*, 52.
(35) Cooper, C. L.; Goulding, A.; Kayitmazer, A. B.; Ulrich, S.; Stoll, S.; Turksen, S.; Yusa, S.-i.; Kumar, A.; Dubin, P. L. *Biomacromolecules* **2006**, *7*, 1025.
(36) Jonsson, M.; Linse, P. *J. Chem. Phys.* **2001**, *115*, 10975.
(37) Jonsson, M.; Linse, P. *J. Chem. Phys.* **2001**, *115*, 3406.
(38) da Silva, F. L. B.; Jönsson, B. *Soft Matter* **2009**, *5*, 2862.
(39) de Vries, R. *J. Chem. Phys.* **2004**, *120*, 3475.
(40) Bendedouch, D.; Chen, S. H. *J. Phys. Chem.* **1983**, *87*, 1473.
(41) Li, Y.; Xia, Q.; Shi, K.; Huang, Q. *J. Phys. Chem. B* **2011**, *115*, 9695.
(42) Kabsch, W.; Sander, C. *Biopolymers* **1983**, *22*, 2577.
(43) Lund, M. Phd Thesis, University of Lund, Sweden. 2006.
(44) Grymonpre, K. R.; Staggemeier, B. A.; Dubin, P. L.; Mattison, K. W. *Biomacromolecules* **2001**, *2*, 422.
(45) Gilson, M. K.; Sharp, K. A.; Honig, B. H. *J. Comput. Chem.* **1988**, *9*, 327.
(46) Stawiski, E. W.; Gregoret, L. M.; Mandel-Gutfreund, Y. *J. Mol. Biol.* **2003**, *326*, 1065.
(47) Davis, M. E.; Madura, J. D.; Luty, B. A.; McCammon, J. A. *Comput. Phys. Commun.* **1991**, *62*, 187.
(48) Marszalek, P. E.; Li, H.; Oberhauser, A. F.; Fernandez, J. M. *Proc. Natl. Acad. Sci. U.S.A.* **2002**, *99*, 4278.
(49) Marcelo, G.; Saiz, E.; Tarazona, M. P. *Biophys. Chem.* **2005**, *113*, 201.
(50) Metropolis, N.; Rosenbluth, A. W.; Rosenbluth, M. N.; Teller, A. H.; Teller, E. *J. Chem. Phys.* **1953**, *21*, 1087.
(51) Norberg, J.; Nilsson, L. *Biophys. J.* **2000**, *79*, 1537.
(52) Bungenberg de Jong, H. G. *Colloid Science*; Kruyt, H. R., Ed.; Elsevier Publishing Co.: Ameterdam, 1949 ;Vol. 2.
(53) Fennema, Q. R. *Food Chemistry*, 3rd ed.; Marcel Dekker, Inc.: New York, 1997.
(54) Yunqi, L.; Zhaoyan, S.; Tongfei, S.; Lijia, A. *J. Chem. Phys.* **2004**, *121*, 1133.
(55) Li, Y.; Sun, Z.; Su, Z.; Shi, T.; An, L. *J. Chem. Phys.* **2005**, *122*, 194909.
(56) Li, Y.; Shi, T.; Sun, Z.; An, L.; Huang, Q. *J. Phys. Chem. B* **2006**, *110*, 26424.
(57) Li, Y.; Shi, T.; An, L.; Lee, J.; Wang, X.; Huang, Q. *J. Phys. Chem. B* **2007**, *111*, 12081.
(58) Kayitmazer, A. B.; Strand, S. P.; Tribet, C.; Jaeger, W.; Dubin, P. L. *Biomacromolecules* **2007**, *8*, 3568.
(59) van der Schoot, P. *Macromolecules* **1998**, *31*, 4635.
(60) Rubinstein, M.; Colby, R. H. *Polymer Physics*; Oxford University Press: New York, 2003.
(61) Sanchez, C.; Renard, D.; Robert, P.; Schmitt, C.; Lefebvre, J. *Food Hydrocolloids* **2002**, *16*, 257.
(62) Shanbhag, S.; Larson, R. G. *Phys. Rev. Lett.* **2005**, *94*, 076001.
(63) Tuinier, R.; Zoon, P.; Olieman, C.; Stuart, M. A.; Fleer, G. J.; de Kruif, C. G. *Biopolymers* **1999**, *49*, 1.
(64) Wang, S. Q.; Ravindranath, S.; Wang, Y.; Boukany, P. *J. Chem. Phys.* **2007**, *127*, 064903.
(65) Wang, X.; Li, Y.; Wang, Y. W.; Lal, J.; Huang, Q. *J. Phys. Chem. B* **2007**, *111*, 515.
(66) Jonsson, M.; Skepo, M.; Tjerneld, F.; Linse, P. *J. Phys. Chem. B* **2003**, *107*, 5511.
(67) Gogelein, C.; Nagele, G.; Buitenhuis, J.; Tuinier, R.; Dhont, J. K. G. *J. Chem. Phys.* **2009**, *130*, 204905.
(68) Verma, R.; Crocker, J. C.; Lubensky, T. C.; Yodh, A. G. *Phys. Rev. Lett.* **1998**, *81*, 4004.
(69) Gögelein, C. *Phase Behaviour of Proteins and Colloid−Polymer Mixtures*, PhD thesis, Mathematisch-Naturwissenschaftlichen Fakultät der Heinrich-Heine-Universität, Düsseldorf, 2008.
(70) Buzzaccaro, S.; Piazza, R.; Colombo, J.; Parola, A. *J. Chem. Phys.* **2010**, *132*, 124902.
(71) Li, Y.; Lee, J.; Lal, J.; An, L.; Huang, Q. *J. Phys. Chem. B* **2008**, *112*, 3797.
(72) Lee, C. T.; Smith, K. A.; Hatton, T. A. *Biochemistry* **2005**, *44*, 524.
(73) Dubin, P. L.; Kayitmazer, A. B.; Seyrek, E.; Staggemeier, B. A. *J. Phys. Chem. B* **2003**, *107*, 8158.
(74) Skepo, M.; Linse, P. *Macromolecules* **2003**, *36*, 508.